

## Deployment and Retraction of a Cable-Driven Solar Array: Testing and Simulation

P. Kumar\* and S. Pellegrino\*

### Abstract

The paper investigates three critical areas in cable-driven rigid-panel solar arrays. First, the variation of deployment and retraction cable tensions due to friction at the hinges. Second, the change in deployment dynamics associated with different deployment histories. Third, the relationship between the level of pre-tension in the closed contact loops and the synchronization of deployment. A small scale model array has been made and tested, and its behavior has been compared to numerical simulations.

### Introduction

Rigid panel solar arrays have been widely and successfully used for Low Earth Orbit missions with power requirements below 10 kW. Their ability to cope with many thermal cycles leads to a longer mission life, while simpler deployment mechanisms ensure reliable operation. In the standard design, for deploy-only missions, these arrays are deployed by a series of torsion springs located at the hinges. The motion of the panels is coupled by a series of synchronization elements, while a damping system attenuates the end of deployment shock. Typical deployment times are around 10 s. The design and analysis of such systems has been studied extensively [1-4].

Cable-driven arrays are used mainly for their retraction capability and to control end-of-deployment shocks more accurately. Typically, two continuous cables run over a series of pulleys connected to the hinges of the solar array. One end of each cable is connected to a motorized drum, whose rotation activates deployment or retraction. The principle of operation is illustrated in Figure 1. In Figure 1(a), a clockwise rotation of the drum shortens the overall length of the deployment cable and hence activates deployment: the angle  $\theta$  increases from 0 to 90 deg. In Figure 1(b), a counterclockwise rotation of the drum shortens the length of the retraction cable and hence causes the solar array to retract, thus decreasing  $\theta$  from 90 to 0 deg. Of course, the deployment cable needs to be lengthened during retraction and, for simplicity, the deployment and retraction cables can be wound on the same drum, but in opposite directions.

For example, a solar array with five full panels and a half-panel or a yoke has six degrees of freedom (dof), of which only one is controlled by the Deployment and Retraction (D/R) cables. The remaining five dof are eliminated by introducing five synchronization elements. A common type of synchronization element is the Closed Contact Loop (CCL), mounted alongside a panel and over two pulleys on either side of that panel. These pulleys are fixed to the outer panels, but are free to rotate relative to the inner one. Thus, the CCL couples the rotation angles of the two outer panels, provided that friction between cable and pulleys is sufficiently large. A chain of five CCL's will remove the five internal dof of the array, thus coupling the motion of panel 1

---

\* Department of Engineering, University of Cambridge, Cambridge, U.K.

to that of the other panels. The remaining global dof, i.e. the rotation of panel 1 with respect to the spacecraft, is controlled by the D/R cable.

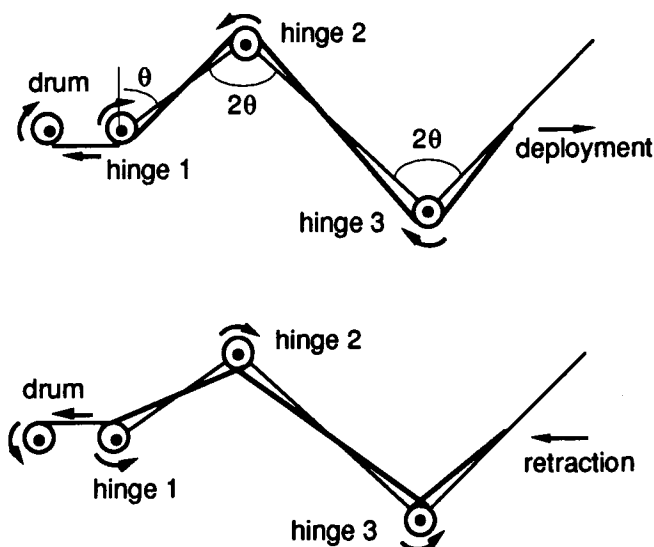


**Figure 1. Operating principle of cable-driven arrays.**

Ideally, each CCL should be highly pre-stressed to avoid slippage, and should also have high axial stiffness for total synchronization. However, a limit on pre-stress is imposed by the buckling load of the panels, while stiffness is limited by the need to control the thermal sensitivity of the system. Often CCL's are mounted in series with springs, whose stiffness is crucial to the dynamic behavior of the solar array.

The objective of this research is to study the D/R behavior of a cable-driven rigid-panel solar array. Three critical areas are investigated. First, the variation of D/R cable tension due to friction at the hinges. Second, the change in deployment dynamics associated with different deployment histories. Third, the relationship between the level of pre-tension in the CCL's and the synchronization of deployment. A small scale, model array has been made and tested, and its behavior has been compared to numerical simulations.

## **Experimental Setup**

### Model array

An accordion type, cable-deployed rigid-panel solar array has been set up. Its design, shown in Figure 2, is a simplified version of the Retractable Advanced Rigid Array used in the European Retrievable Carrier (EURECA) [5, 6]. The model array consists of one half-length panel and five full-length, 16 gauge (1.63 mm thick) Al-alloy panels. The panels are connected to each other and to horizontal brackets, bolted to a vertical plate, by continuous stainless steel shafts with radius  $r = 3$  mm. All connections are through Al-alloy hinge assemblies, Figure 3(a), whose PTFE lined journal bearings have a friction coefficient  $\mu = 0.15$ . Two multi-stranded steel cables, one for deployment and

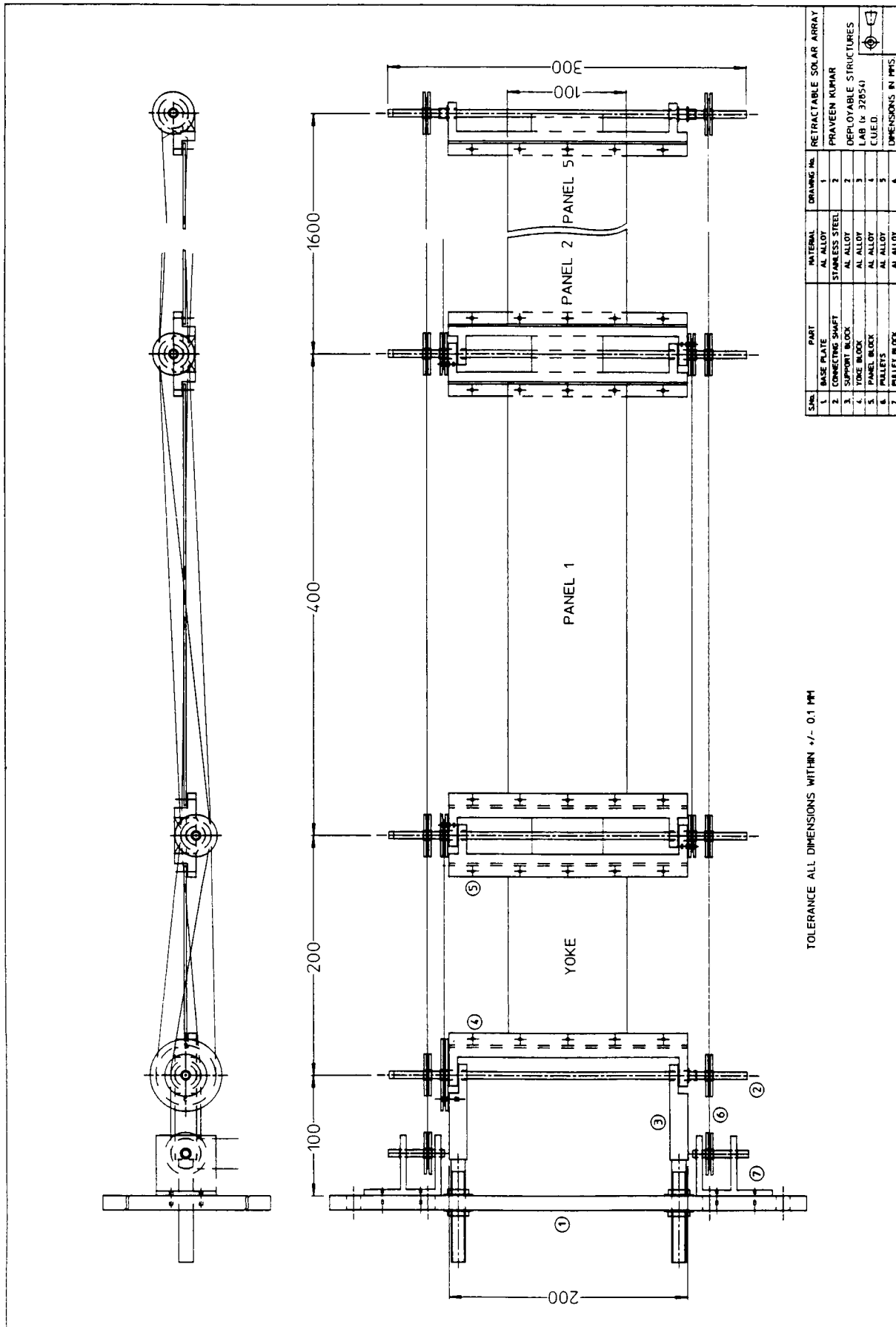
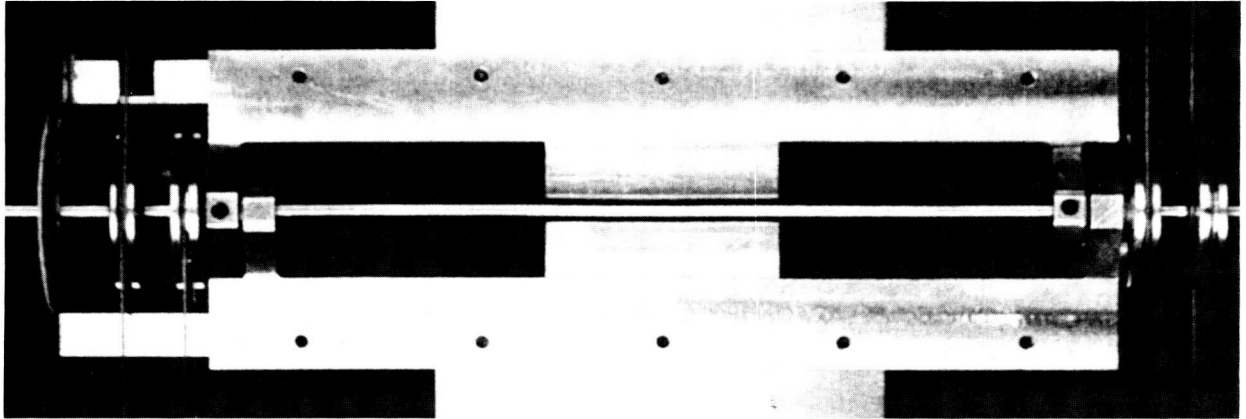
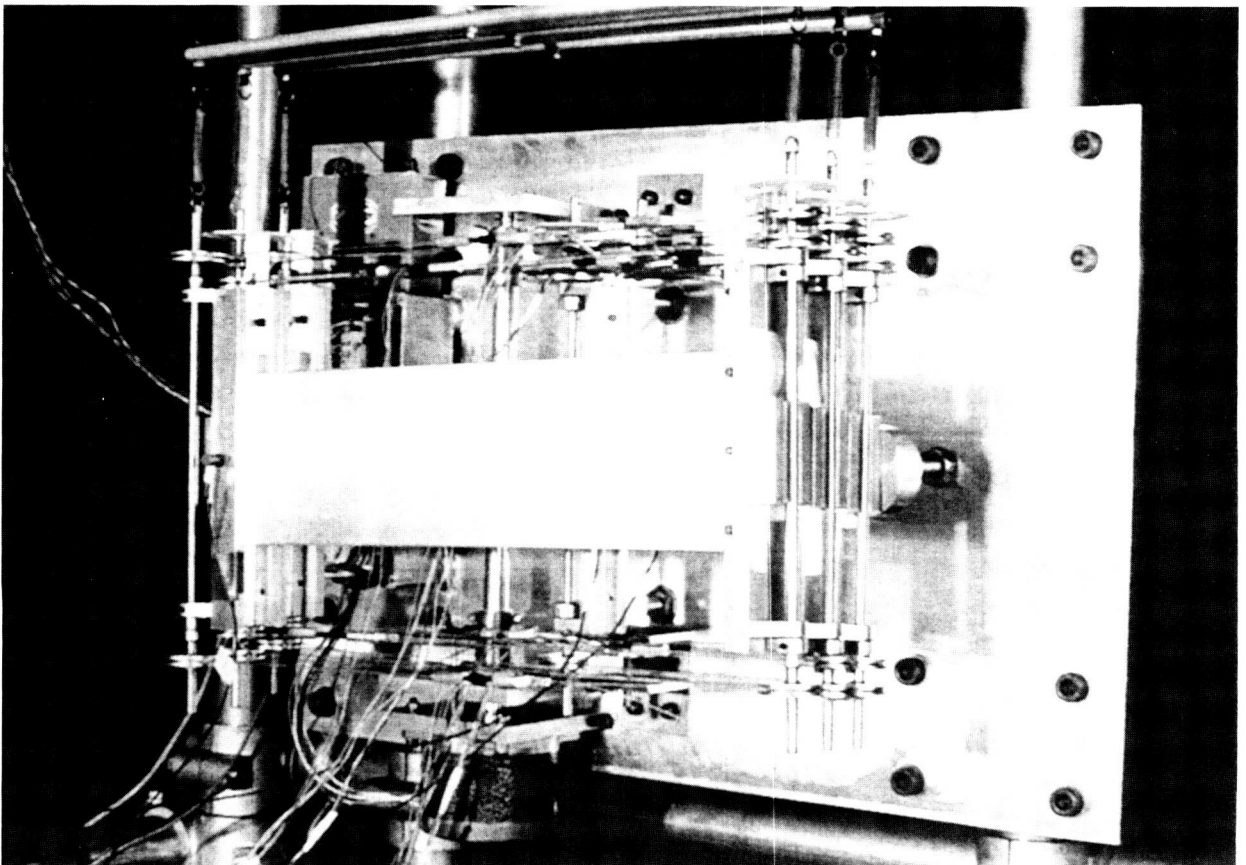


Figure 2. Schematic drawing of the model array.



(a)



(b)

**Figure 3. (a) Hinge detail. (b) View of array.**

one for retraction, are mounted on either side of the panels. Each cable has diameter of 0.8 mm and breaking load of 54 N, and runs over a series of pulleys with radius  $R = 12.5$  mm. These pulleys are mounted on the hinge shafts with the same journal bearings described above. The D/R cables are connected to a single drum, bolted to the vertical mounting plate shown on the left hand side of Figure 3(b). Five CCL's, each consisting of a multi-stranded steel cable in series with a soft spring, synchronize the motion of the panels. Each CCL applies a compressive axial force on the panel, whose magnitude is equal to double the pre-tension in the loop. The thickness of the panels is sufficiently large to avoid buckling, and yet the vibration of the array during D/R is appreciable. The total mass of the model array is 4.2 kg, mainly concentrated at the hinges. It is supported by a gravity compensation system consisting of three independent linear bearings running on horizontal rails. Each bearing is connected to two hinge shafts and has a mass of 0.1 kg.

### Stepper Motor

Stepper motors offer many advantages over DC torque motors for space applications [7]. Particularly relevant to this study is their ability to follow accurately any prescribed D/R profile by simple open loop control. To eliminate positioning errors due to backlash, the motor has been connected directly to the drum, without any reduction gears. A well-known disadvantage of standard stepper motors without gears is the relatively large size of each step, a full revolution is usually divided into 200 steps, and hence one step corresponds to 1.8 deg, which results in a very irregular motion. However, each full step can be sub-divided into up to 256 steps using a microstepping drive, with the only disadvantage of reducing the available torque by up to 30%.

To estimate the maximum torque required from the stepper motor, the maximum difference between the tension in the deployment and retraction cables is required.

Assuming, for simplicity, a uniform tension  $F$  in the deployment cable, no tension in the retraction cable, and a uniform pre-tension  $S$  in all CCL's, the work done on the system must be equal to the energy dissipated by friction, for any small configuration change of the array. For a small rotation  $d\theta$  of all panels, this gives

$$11RF d\theta = 82 \mu r F \cos \theta d\theta + (44 \cos \theta + 16) \mu r S d\theta \quad (1)$$

$$F = \frac{(44 \cos \theta + 16) \mu r S}{11R - 82 \mu r \cos \theta} \quad (2)$$

For  $r = 3$  mm,  $R = 12.5$  mm,  $\mu = 0.15$ ,  $S = 30$  N and  $\theta = 90$  deg, Equation 2 gives

$$F = 7.2 \text{ N}$$

Because there are no latches in this type of solar array, at the end of deployment the tension in the deployment cable has to be increased to 25 N to prevent hinge line gapping. Thus, with a drum radius of 10 mm a torque of 250 N•mm is required to deploy and pretension the array. Using a torque margin of 4, and an additional 30% for the microstepping drive, a final motor torque of 1.3 N•m is arrived at. Note that the motor torque requirement is linked to the final level of pre-tension of the array; the torque required for deployment is much lower.

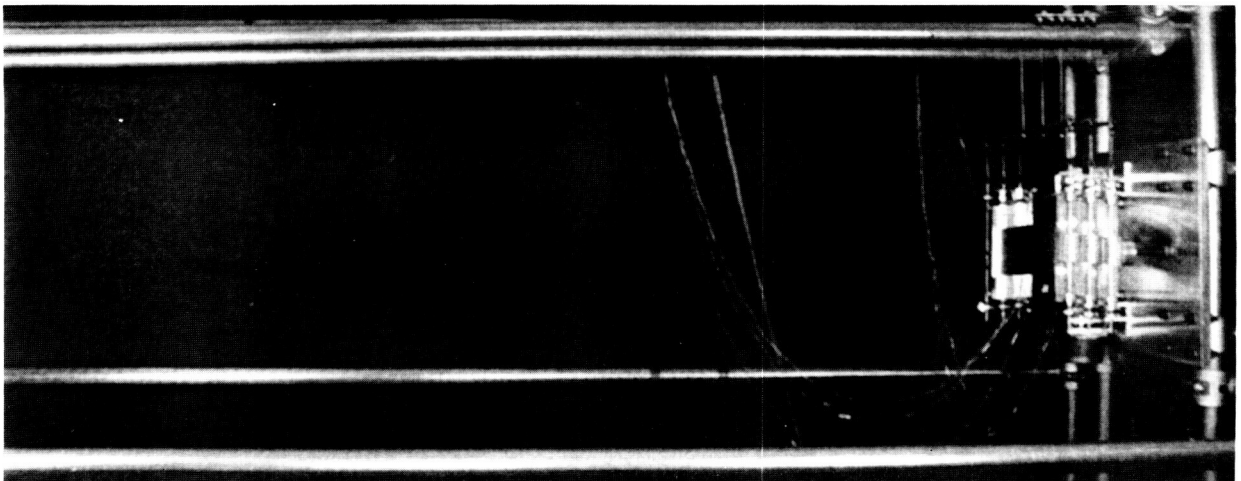
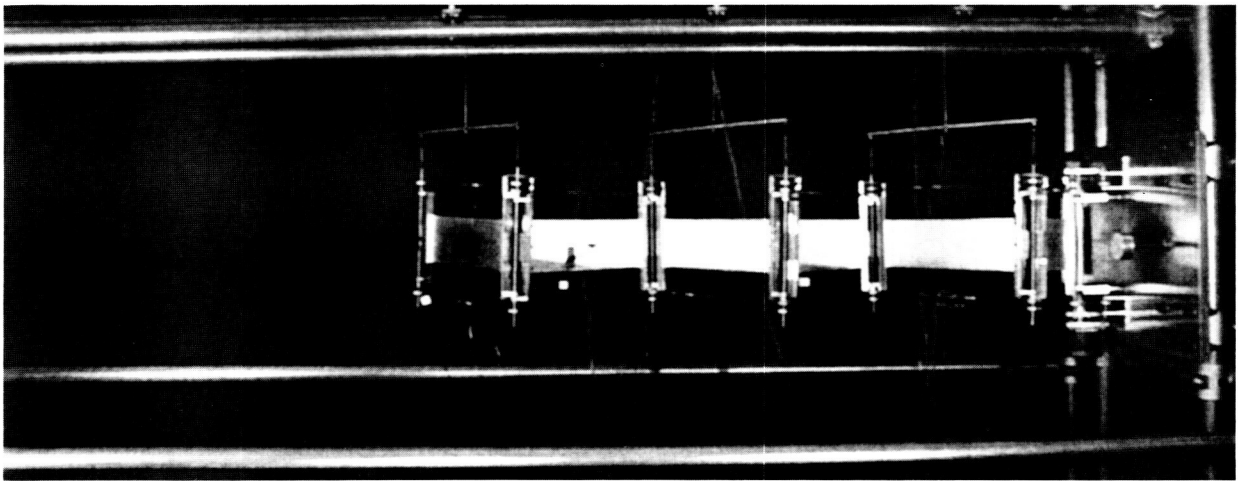
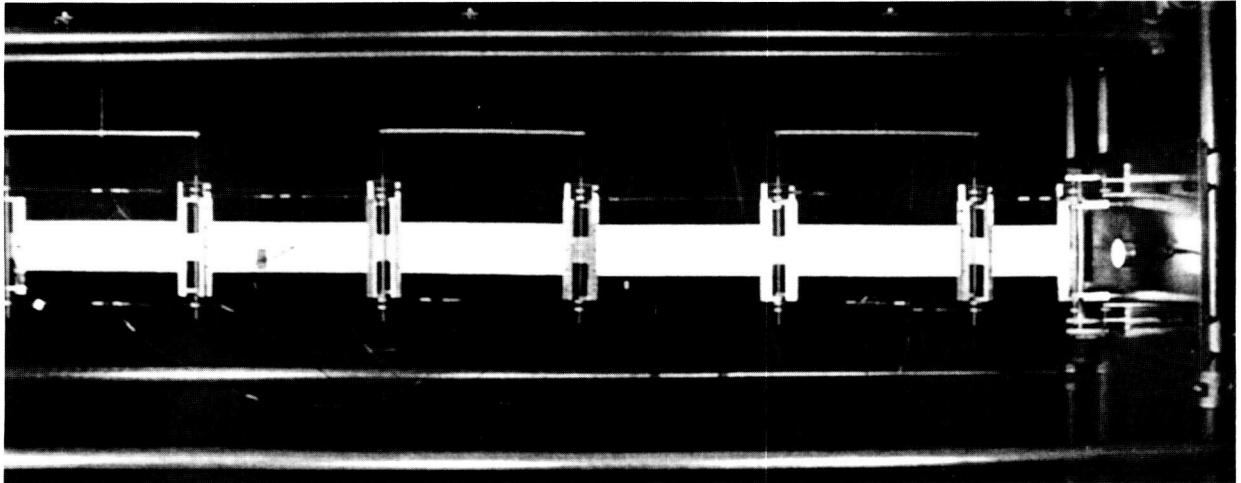
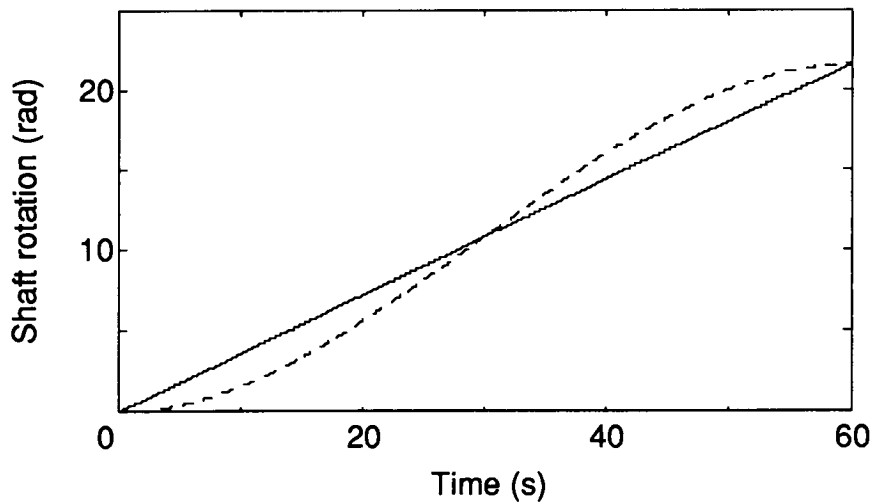


Figure 4. Retraction sequence.

A SMS 341-044 hybrid stepper motor has been chosen with a nominal torque capacity of 1.3 N·m @ 300 rpm. The motor is driven by a CMM 542 microstepping drive, set at 12800 steps/revolution and connected to a personal computer through a multi-function digital-analog converter board (Amplicon PC-30PGL). The board outputs a pulse each time the motor is required to turn through one step.

A constant angular speed of the drum is obtained by sending a series of pulses at a constant frequency, while a variable speed requires the pulse frequency to be varied accordingly. The drum rotation profiles that have been used in the experiments are shown in Figure 5. Note that the linear profile involves a sudden acceleration / deceleration of the array when the motion starts/stops, while the non-linear profile, a third-order polynomial with zero slope at the start and at the end is much smoother.



**Figure 5. Linear and non-linear drum rotation profiles.**

### Instrumentation

The instrumentation of the model array includes three types of transducers. Strain gauges, glued on turnbuckles, measure the tensions  $D_{2\_3}$ ,  $D_{6\_7}$ ,  $R_{2\_3}$ ,  $R_{6\_7}$ , respectively in the deployment and retraction cables, and between hinges 2-3 and 6-7. Pairs of strain gauges are mounted also on the CCL's between hinges 2-3 and 5-6. The torques applied by these CCL's respectively onto hinges 3 and 6 are obtained by multiplying the change of tension in each side of a CCL by the pulley diameter. These torques are positive if anti-clockwise. A Quartz Shear Mode ICP Accelerometer, mounted at the tip of the array, monitors vibrations. Finally, an angular dial gauge is attached to each hinge shaft, to monitor panel rotations.

### **Test Results**

D/R tests have been performed for different drum rotation profiles, total deployment times, and CCL pre-tensions. This section presents a complete set of results obtained from a reference test, where the D/R time is  $T = 60$  s, the drum rotation profile is a linear ramp, and  $S = 30$  N. The behavior of the array during this test is compared to the

response when  $T = 30$  s, when the rotation profile is non-linear, and when the CCL pre-tension is reduced to 15 N.

#### T = 60 s: Linear Ramp: S = 30 N

The results from the deployment test are shown in Figure 6. The tensions in the deployment and retraction cables, Figure 6(a, b), show very similar patterns. At the start  $D_{2\_3} \cong D_{6\_7} \cong 3$  N and  $R_{2\_3} \cong R_{6\_7} \cong 30$  N. As the array starts to deploy, the cable tensions rapidly converge to  $D_{2\_3} \cong 12$  N,  $D_{6\_7} \cong R_{6\_7} \cong 9$  N, and  $R_{2\_3} \cong 4$  N. The tension in the deployment cable decreases from the drum towards the tip of the array, while the tension in the retraction cable increases. Finally, as the array reaches its fully deployed shape, the tension in the deployment cable quickly increases until the motor stops. The torques applied to hinge 3 and hinge 6 are shown in Figure 6(c), assuming that all synchronization torques are zero at the start. The torque applied by CCL<sub>2\_3</sub> is of greater magnitude and of opposite sign to that applied by CCL<sub>5\_6</sub>. There is no simple pattern in the variation of these torques, and no simple correlation between them.

The results from the retraction test are shown in Figure 7. The role of the deployment cable is similar to the role of the retraction cable in the earlier test. Hence, now  $D_{2\_3} \cong 5$  N and remains approximately constant throughout, while  $D_{6\_7}$  varies in the range 8-9 N. The tension in the retraction cable, though, increases steadily and  $R_{2\_3} > R_{6\_7}$ . Both torques applied by the instrumented CCL's vary with similar patterns and in the same range, approximately -100 to 0 N, but in opposite directions. CCL<sub>2\_3</sub> quickly drops to about -100 N•mm at the start and gradually increases, before dropping to about -150 N•mm towards the end of the test. CCL<sub>5\_6</sub> starts at zero and gradually decreases to -100 N•mm. As in the deployment test, these torques have been set equal to zero at the start; note that they are not zero at the end.

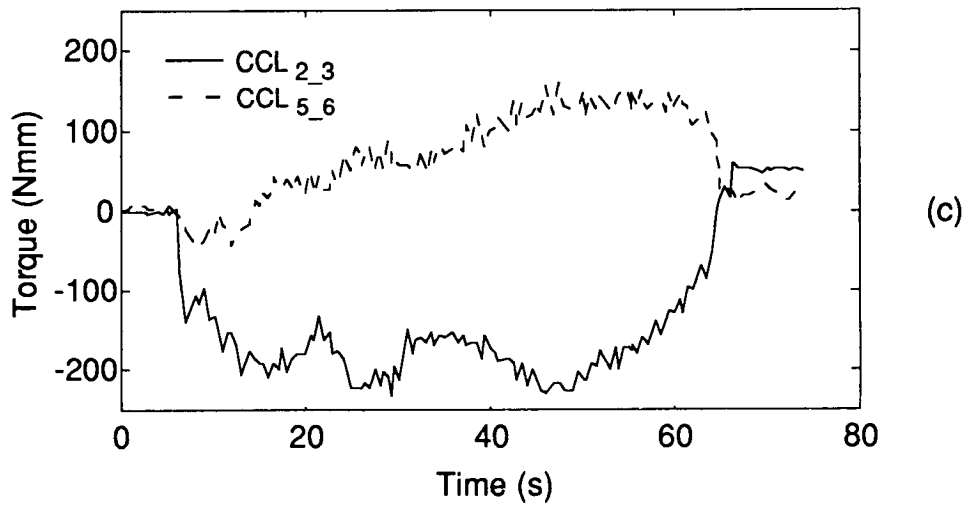
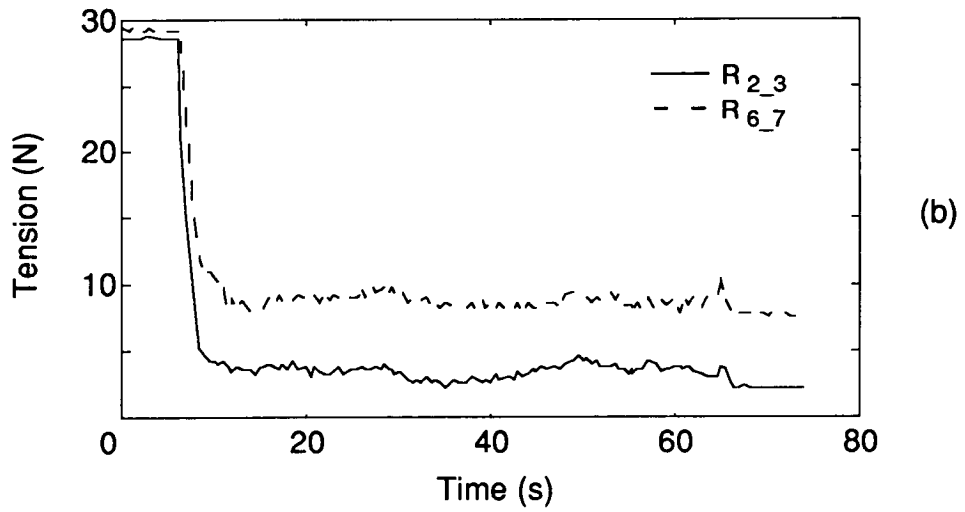
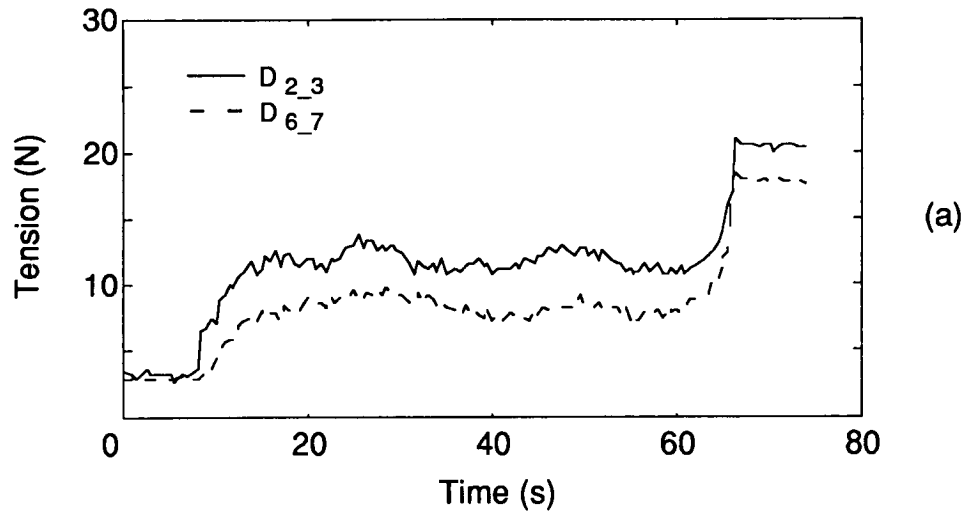
#### T = 60 s: Non-Linear Ramp: S = 30 N

Figure 8(a) compares the variation of  $D_{2\_3}$  in the reference deployment test with the response obtained using the smoother drum rotation profile shown in Figure 5. The differences are quite small, and mainly due to the way the data is plotted. The tension builds up to its (approximately) steady-state value at a slower rate because during the first half of the test  $\theta$  lags behind the reference test. Towards the end of the test, though,  $\theta$  leads the reference test and hence the end-of-deployment tension increase occurs earlier. The two curves practically coincide if tension is plotted as a function of  $\theta$ , instead of time.

The important difference between this and the standard test is that the shock loading of the array at the start and end of deployment is much lower. Figure 8(b, c) shows plots of accelerometer data taken at a constant sampling rate of 50 Hz. The 1 g acceleration peaks measured in the reference test have now been eliminated.

#### T = 30 s: Linear Ramp: S = 30 N

Halving the deployment time has no significant effects on  $D_{2\_3}$ , but leads to larger shocks at the start and end of deployment.



**Figure 6. Deployment in 60 s, linear ramp.**

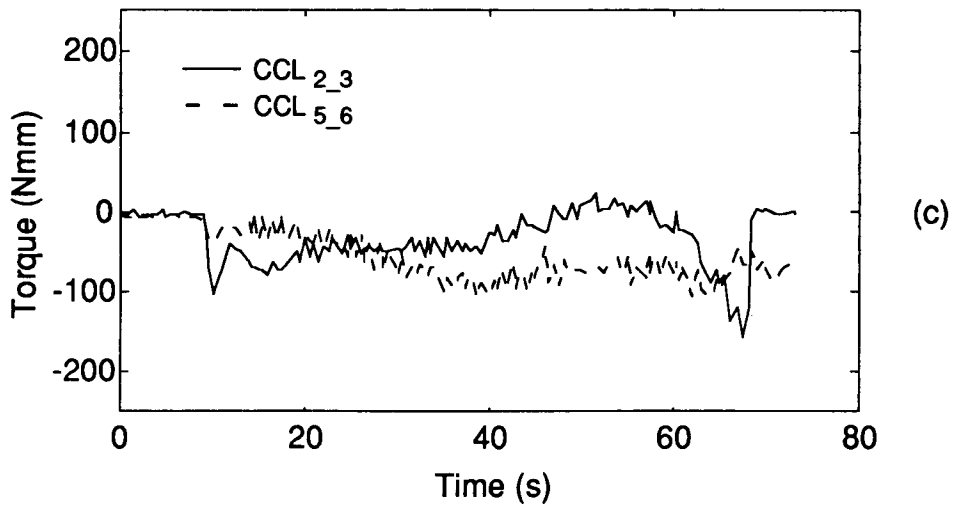
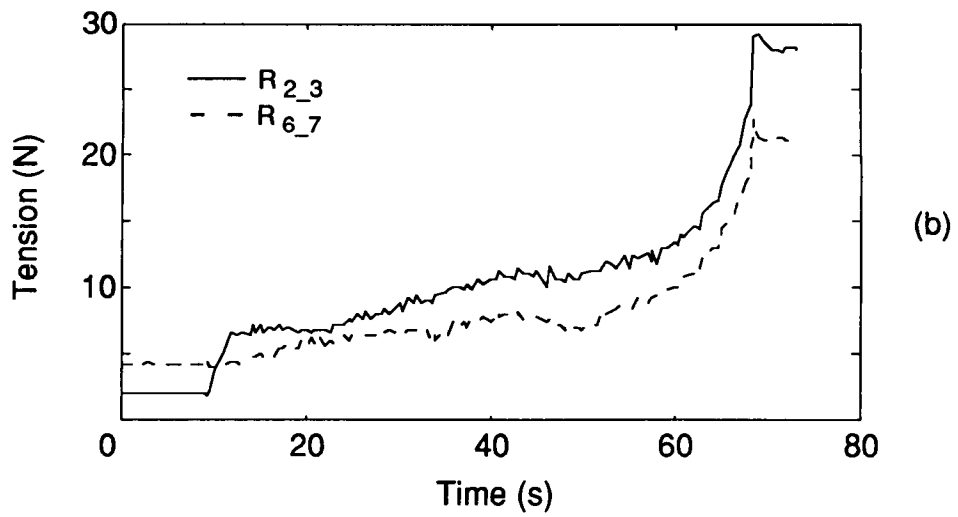
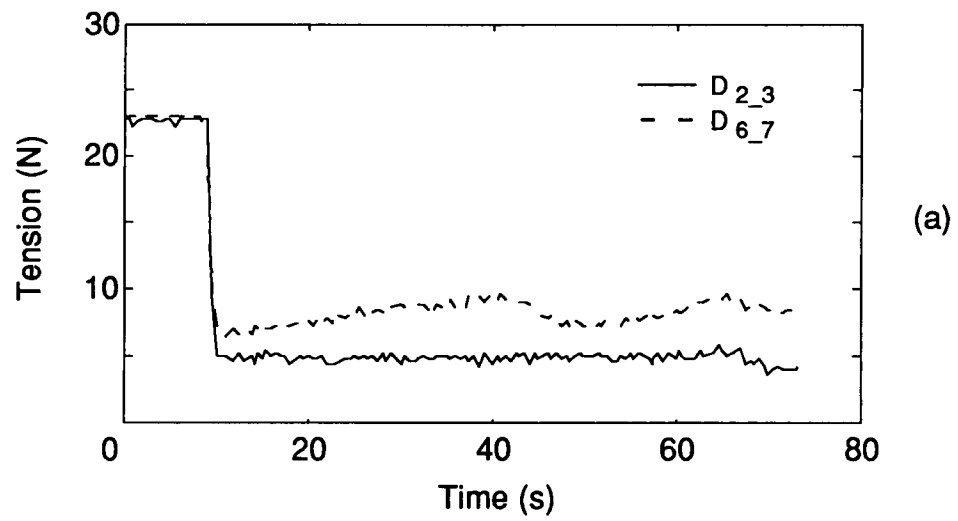


**Figure 7. Retraction in 60 s, linear ramp.**

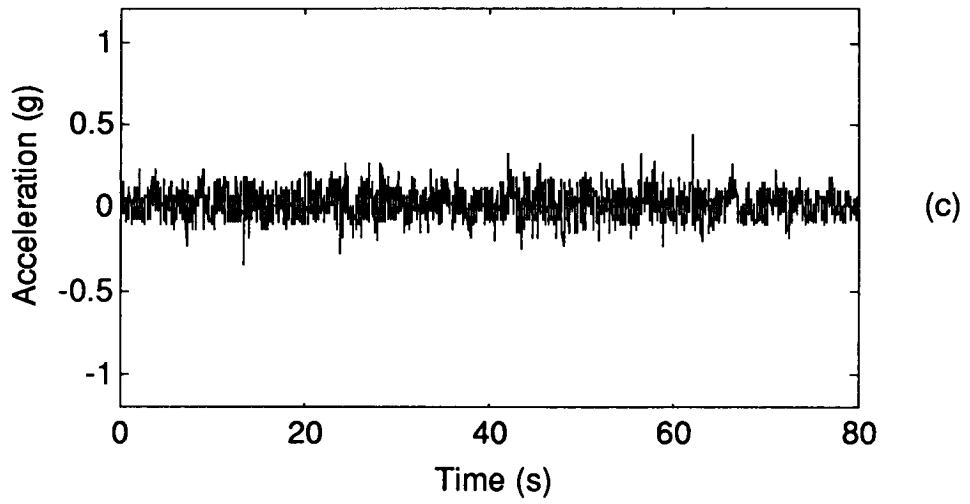
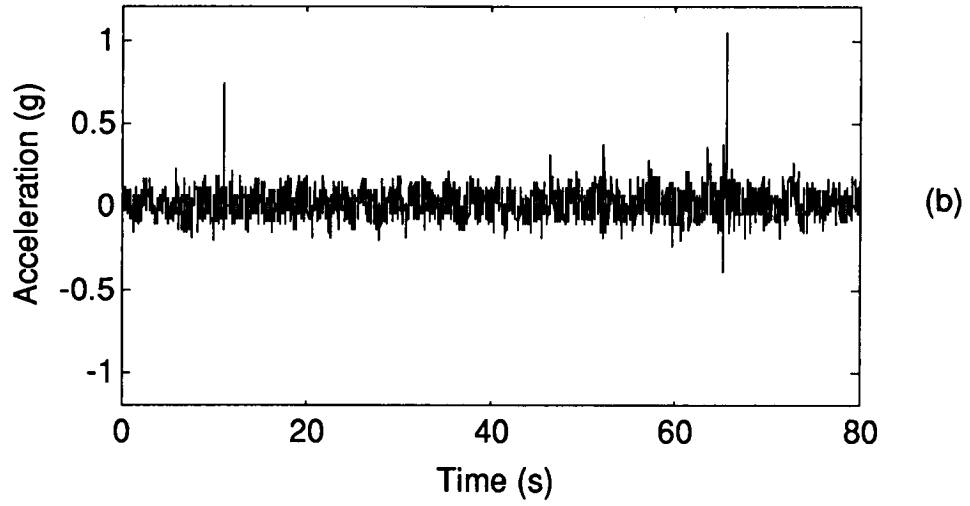
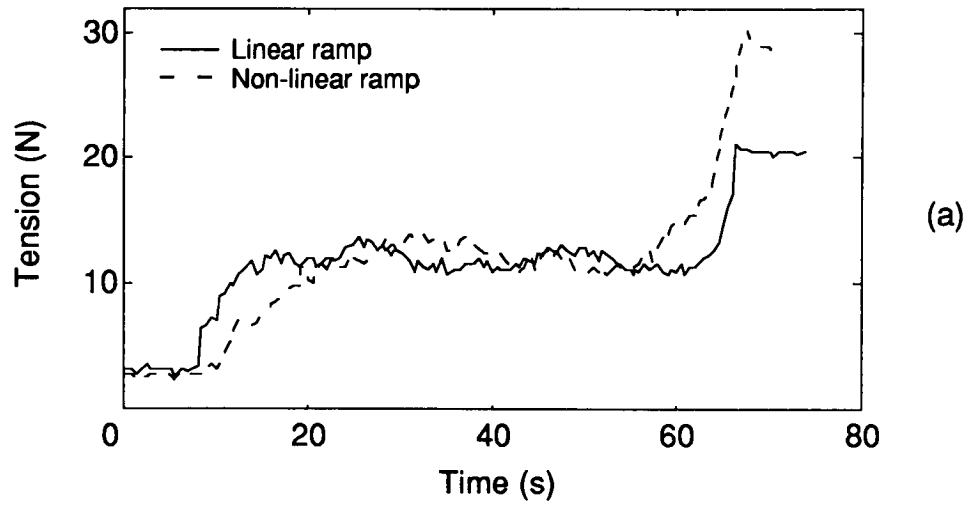


**Figure 8. Comparison of linear vs non-linear ramp.**

T = 60 s: Linear Ramp: S = 15 N

In the reference test there is good synchronization between different panels. Figure 9(a) shows that all hinge rotations are within  $\pm 5$  deg of their nominal values, i.e.  $\theta$  for hinge 1 and  $2\theta$  for hinges 2-6. If the CCL pre-tension is reduced to  $S = 20$  N, the array is still well synchronized. If the pre-tension is further reduced to  $S = 15$  N there is a substantial loss of synchronization, see Figure 9(b). Hinges 5 and 6 are now *lagging* i.e. they have turned through an angle smaller than  $2\theta$ , whereas hinges 1 and 2 are *leading*.

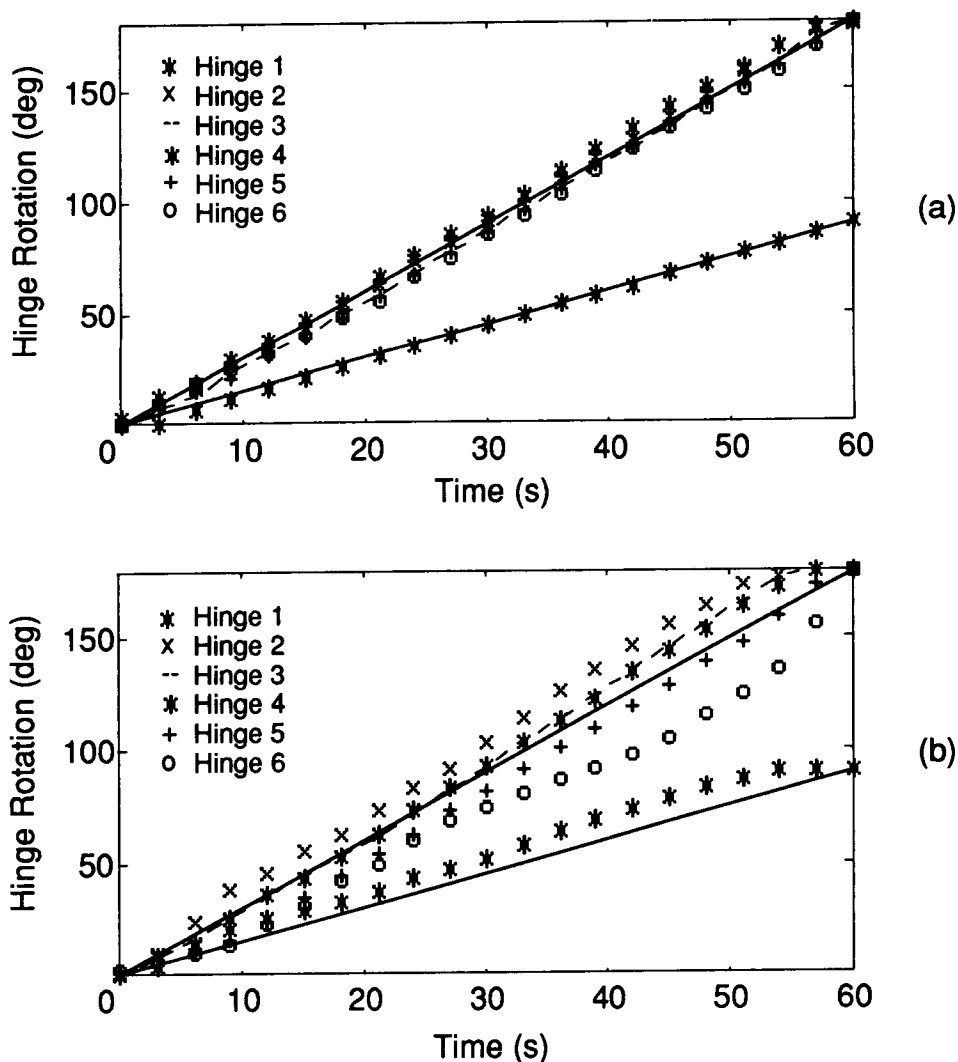


**Figure 9. Hinge synchronisation for different CCL pre-tension (a) 30 N; (b) 15 N.**

## Simulations

A model of the solar array has been set up using ADAMS [8], a multi-body dynamic analysis package which has been used for solar array deployment simulations [9].

The model consists of a two-dimensional chain of elements, connected by hinges. Each element simulates a panel, whose elastic properties are modelled by the stiffness matrix of a corresponding BEAM element. A frictionless pulley of radius  $R$  is connected to each hinge. The D/R cable is modelled using a SFORCE element, which applies a tangential force to the pulley connected to hinge 2. At any stage of the calculation, the magnitude of SFORCE is equal to the current length of the D/R cable, including the length wound onto the drum, less the initial length, multiplied by the axial stiffness of the cable. Synchronization between different panels is imposed by applying a series of torques to the hinges. Each torque is equal to the difference between the rotation angles of adjacent panels, multiplied by  $2R$  times the axial stiffness of the cable. The effects of friction are simulated by applying frictional torques at all hinges.

A simpler, purely kinematic model of the array has also been developed, where five hinge rotations are coupled to MOTION GENERATORS.

Figure 10 shows a simulation of the retraction process, obtained from the kinematic model. Obtaining sensible results from the more complex dynamic model has proved quite difficult. If realistic values of the mass and stiffness properties are used, the calculations become very sensitive to initial conditions and small errors, and therefore it is impossible to achieve the correct motion pattern. So far, the correct motion pattern has been obtained only from dynamic models with very low mass and stiffness.

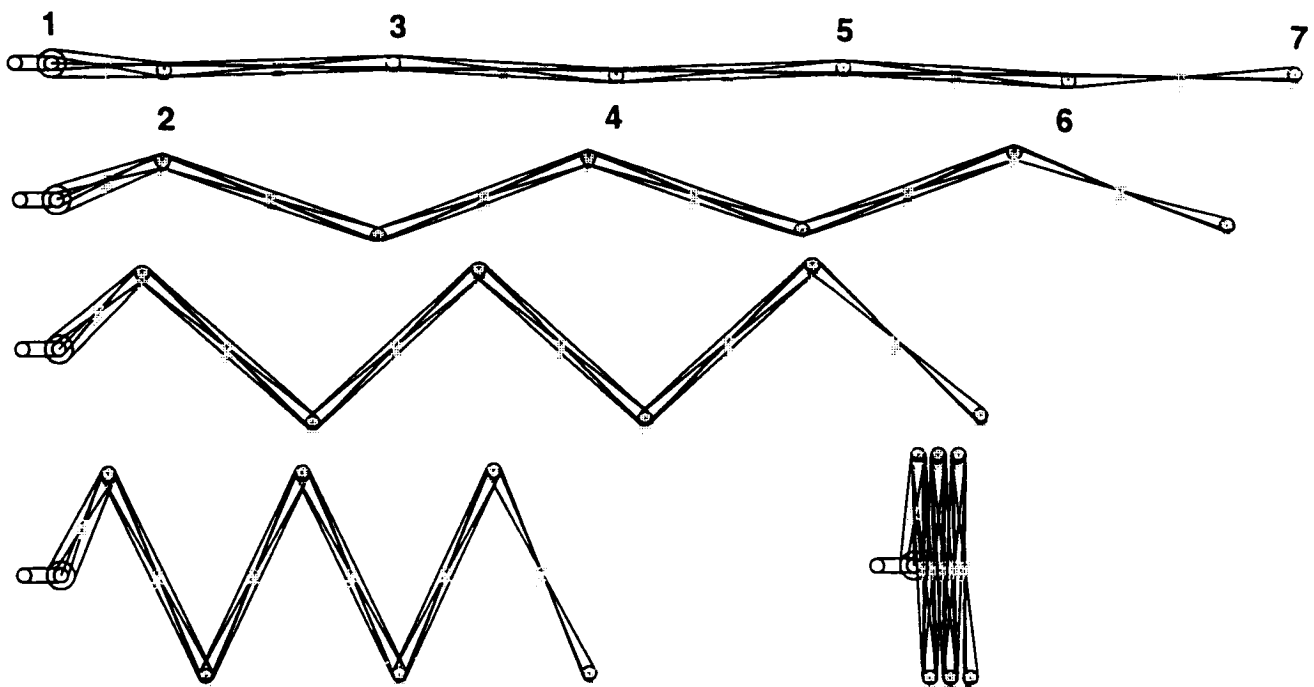


Figure 10. ADAMS simulation of retraction.

An alternative, quasi-static model of the array D/R process has been developed. It is assumed that all accelerations are sufficiently small to be negligible, and that limiting friction is reached simultaneously at all hinges. Therefore, tensions in the deployment cable can be obtained from a single value, e.g.  $D_{0\_1}$ , while the tensions in the retraction cable can be obtained from  $R_{0\_1}$ . These assumptions are believed to be reasonable in a simulation of a slow D/R process that neglects the initial and final transients.

During deployment, for any configuration of the array and for any given value of  $R_{0\_1}$ , the forces and moments in each panel are related to the torques applied by the CCL's and to  $D_{0\_1}$  by a non-linear system of equilibrium equations. A complete description of this analytical model will be published elsewhere. Figure 11 shows the predicted behavior of the array, obtained by solving the above system of equations for many values of  $\theta$ , and for  $R_{0\_1} = 6\text{ N}$  and  $S = 30\text{ N}$ .

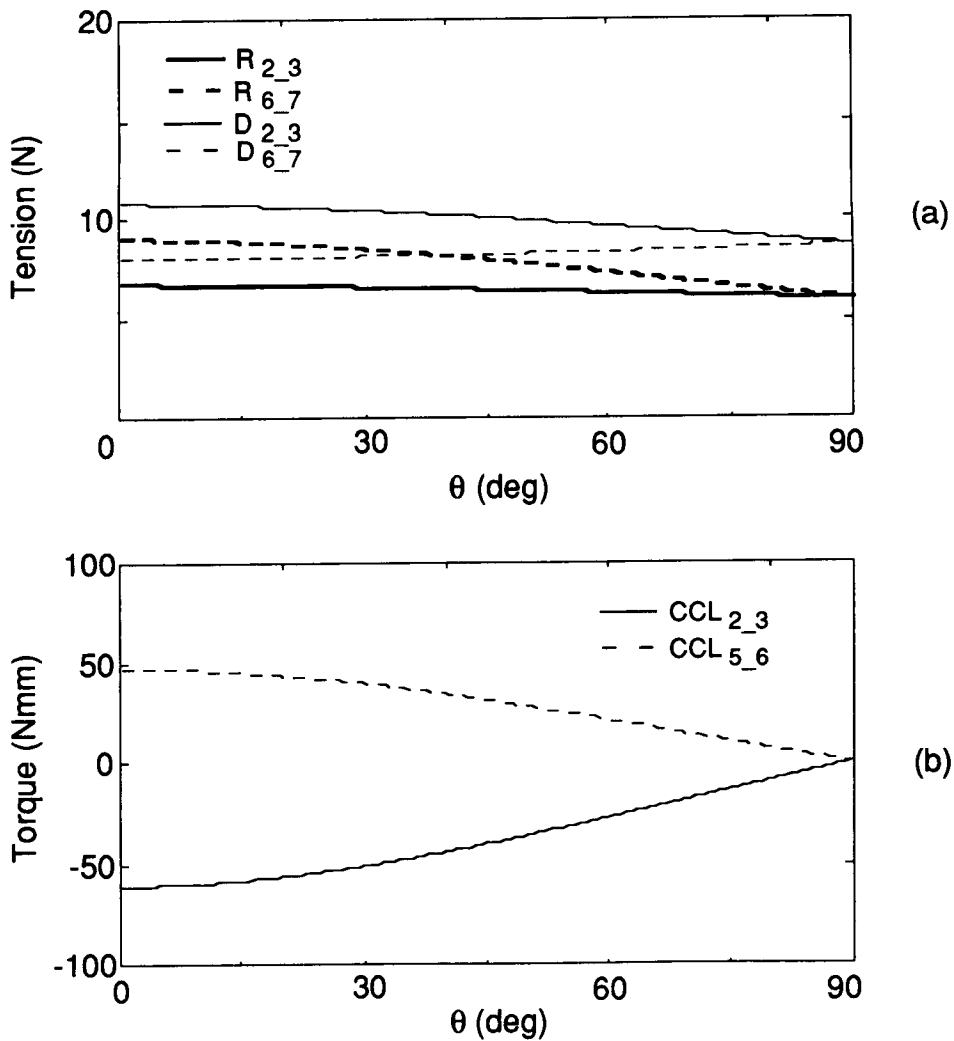


Figure 11. Analytical predictions of solar array behaviour during deployment.

A similar analysis of the retraction process has given almost identical results, but the tensions in the D/R cable are exchanged, and the sign of the CCL torques are reversed.

## Discussion

The model array has shown, unexpectedly, significant differences in behavior between deployment and retraction. During deployment, the tensions in the D/R cables remain roughly constant, which is consistent with the simulation results. During retraction, though, the tension in the retraction cable steadily increases, which is not shown by the simulations. Also, significant differences have been observed in the variation patterns, as well as in the magnitudes of the synchronization torques applied by the CCL's. Thus, while there is a reasonably good correlation between the simulations and the torques measured during retraction, the agreement is poor for the deployment data. These discrepancies are not caused by inertia forces, neglected in the simulations, because almost the same response is measured when the array is deployed and retracted at much lower speeds. An alternative explanation is that in the present set-up there is an undesired coupling between array and gravity-compensation system, which is quite flexible. A stiffer system is being considered.

## Acknowledgment

P. Kumar gratefully acknowledges financial support from the Cambridge Commonwealth Trust.

## References

1. Vorlicek, P.L., Gore, J.V. and Plescia, C.T. "Design and Analysis Considerations for Deployment Mechanisms in a Space Environment." *16th Aerospace Mechanisms Symposium* (May 1982), pp. 211-222.
2. Wie, B., Furumoto, N., Banerjee, A. K. and Barba, P. M. "Modeling and Simulation of Spacecraft Solar Array Deployment." *AIAA Journal of Guidance Control and Dynamics*, 9, (1986), 593-598.
3. Nataraju, B. S. and Vidyasagar, A. "Deployment Dynamics of Accordion Type of Deployable Solar Arrays Considering Flexibility of Closed Control Loops." *Proceedings of 38th IAF Congress* (1987).
4. Celli, J., Lomas, N., Pollard, H. and Totah, N. "Intelsat VII Solar Array Electrical and Mechanical Design." *Proceedings of 13th AIAA International Communication Satellite Systems Conference and Exhibition*, (March 1990), pp 34-41.
5. de Kam, J. "EURECA Application of the RARA Solar Array." *Proceedings of Photovoltaic Generators in Space* (October 1986), ESA, pp 105-114.
6. Racca, G. D., Bongers, E. and Sebek, R. "Solar Array Mechanism Design and Performance." *Proceedings of EURECA Symposium*, (April 1994), pp 223-229.
7. Hinkle, K. "Spacecraft Deployable Appendages." NASA Goddard Space Flight Center Report, May 1992.
8. Mechanical Dynamics. "ADAMS Reference Manual Version 7.0." 1993.
9. Roux, C. and Flament, P. "Solar Array Deployment Simulation Using ADAMS Software." *Proceedings of Second European Mechanisms & Tribology Symposium* (October 1985), pp 41-46.